INTERNATIONAL JOURNAL OF PRECISION ENGINEERING AND MANUFACTURING Vol. 19, No. 6, pp. 837-848 JUNE 2018 / 837

REGULAR PAPER

DOI: 10.1007/s12541-018-0100-5
ISSN 2234-7593 (Print) / 2005-4602 (Online)

Mathematical Model and Tooth Contact Analysis of an Internal Helical Gear Pair with Selectable Contact Path

Shuai Peng[1], Bing-kui Chen[1], Dong Liang[1,#], Lu-he Zhang[1], and Si-ling Qin[1]

1 State Key Laboratory of Mechanical Transmission, Chongqing University, No. 174, Shazheng Street, Shapingba, Chongqing, 400044, China
Corresponding Author / E-mail: liangdong213@cqu.edu.cn, TEL: +86-23-65106247
ORCID: 0000-0002-9956-7634

KEYWORDS: Internal gear, Point contact, Mathematical model, Tooth contact analysis, Selectable contact path

An internal helical gear pair with point contact pattern based on the space meshing theory is proposed which consists of an involute internal gear and a pinion with quadratic curve profile. Particularly, the contact path of the tooth surface is selectable, which can inherit the characteristic of the surface. Moreover, this type of internal gear pair has lower sensitivity to assembly errors. The generation principle and mathematical model is presented. The motion simulation and adaptability to center distance error of the internal gear pair are discussed. The gear pair is manufactured. Based on the mathematical model and tooth contact analysis (TCA) method, the locations of contact points and kinematic errors are determined under different center distance variation and axial misalignments. The simulated results reveal that the locations of contact points of the gear and pinion change under assembly errors. Little kinematic error occurs under axial misalignment. No edge contact occurs under any assembly error condition. Experiment study is performed and the result is consistent with the theoretical analysis.

Manuscript received: June 5, 2017 / Revised: February 12, 2018 / Accepted: February 20, 2018

NOMENCLATURE

u, v = parameters of the surface
ϕ = parameter of the space curve
$\mathbf{M}_{ij}$ = transformation matrix from system j to i
t = parameter of curve Γ_c
r =radius of base circle
θ =involute parameter
p = helix parameter
α = rotation angle about the axis
B = tooth width
i_{12} = transmission ratio
k_1 = parameter of quadratic curve
z_1, z_2 =teeth numbers of pinion and internal gear
$\Delta\phi_2$ = kinematic error of the gear pair

1. Introduction

Internal gear pair has been widely applied in gear boxes such as planetary mechanisms, aerospace and differential mechanisms due to the advantages of low contact stress and high contact ratios compared with external gear pair.[1]

As for contact pattern of internal gears, line contact pattern is the most commonly used. Involute gears are applied all over the world because of the convenience of manufacturing and low assembly accuracy.[2] Gears with point contact pattern have been developed over the decades. They have the advantages of high contact strength, high efficiency and low noise. In particular, as for internal gears, Zhang[3] provided a new method of calculating the profile of the gear tooth of the straight conjugate internal meshing gear pump. Xu[4] proposed a double-circular-arc gear with inner meshing. Kahraman[5] investigated the effect of flexibility of an internal gear on the quasi-static behavior of a planetary gear set. Tunalioglu and Tuc[6] investigated the wear in internal gears at different conditions by using Archard's wear modified equation and a MATLAB program.

Assembly errors such as center distance variation and axial misalignment always take place in the process of gear transmission. Due

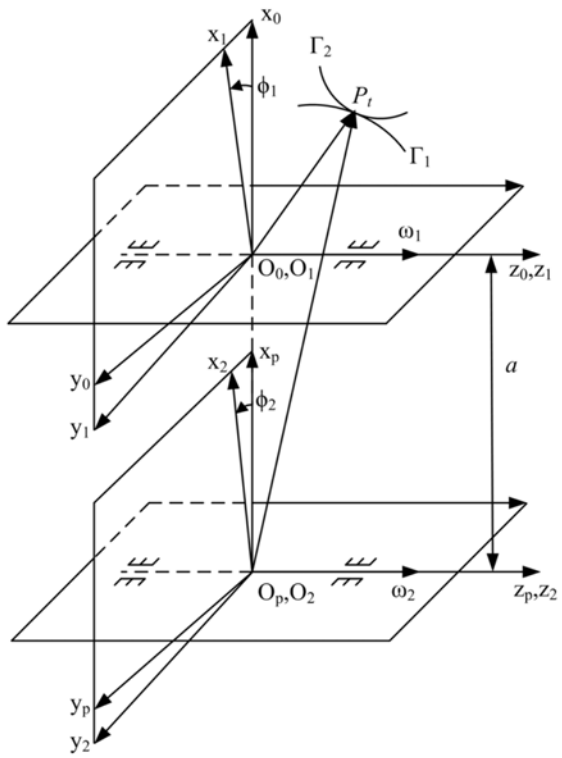

Fig. 1 Coordinate systems

to the characteristic of center distance adaptability, involute gears are not sensitive to center distance variation. However, axial misalignment will cause edge contact and high contact stress on local area.[7,8] This unfavorable engagement behavior will lead to harmful vibration and unwanted noise or even gear failure. By now, some researches concerning the problem have been carried out. Hua[9] investigated the influence of alignment errors on straight bevel gear and analyzed the contact pressure under various alignment errors according to the Archard wear relationship. Deng[10] analyzed the distributions of kinematic error and tooth surface contact stress and shear stress under different installation errors according to the tooth segment topology modification equation. Lim[11] analyzed the influences of assembly error and bearing elasticity on the spur gear dynamic behavior. Tang[12] researched the change rules of kinematic error of hypoid gear and contact path under various errors. Shen[13] proposed a method for the face-gear addendum contacts with the tooth face of a spur gear, and the tooth edges points was determined. Moreover, tooth modification such as lead crowning and tooth profile modification was applied to lower the sensitivity of axial misalignment.[14-16] However, in spite of the above-mentioned studies, few efforts have been directed at meshing principle and geometry design to improve the situation.

This paper proposes an internal gear pair with point contact pattern based on the space meshing theory. This type of gear pair has the advantage of adaptability to assembly errors. The generation principle and mathematical model of the internal gear pair is presented. The gear pair consists of an internal gear and a pinion with quadratic curve tooth profile. Particularly, the contact path of the tooth surface is selectable, which inherits the characteristic of the surface and provides more flexibility and diversity for gear designing. Then, the meshing characteristics of the internal gear pair are discussed. Based on the mathematical model and tooth contact analysis (TCA) method,[17] the locations of contact points and kinematic errors are determined under different center distance variations and axial misalignments. Motion simulation and experiment study are performed to investigate the transmission performance with assembly errors. The conclusions are provided at the end of the paper.

2. General Principle of Gear Mesh

2.1 Geometric model of gear mesh

Coordinate systems are shown in Fig. 1. Fixed coordinate systems $S_0(O_0\text{-}x_0, y_0, z_0)$ and $S_p(O_p\text{-}x_p, y_p, z_p)$ are rigidly connected to the absolute space. Movable coordinate systems $S_1(O_1\text{-}x_1, y_1, z_1)$ and $S_2(O_2\text{-}x_2, y_2, z_2)$ are rigidly connected to the pinion and the gear, respectively. The pinion rotates around axis z_0 with an instantaneous angular velocity ω_1 while the gear rotates around axis z_p with an instantaneous angular velocity ω_2. Axis z_p and z_p are two parallel lines and O_0O_p is the minimum distance, i.e. the center distance a. Angles ϕ_1 and ϕ_2 are the angular displacements of the pinion and the gear, respectively. Point P_t is the contact point of curve Γ_1 and surface Σ_2.

Assuming that the equation of the given surface Σ_2 in movable coordinate system S_2 is

$$\Sigma_2^2 = x_2(u,v)\boldsymbol{i}_2 + y_2(u,v)\boldsymbol{j}_2 + z_2(u,v)\boldsymbol{k}_2 \tag{1}$$

where $x_2(u, v)$, $y_2(u, v)$, $z_2(u, v)$ are the scalar functions of u, v, $\boldsymbol{i}_2$, $\boldsymbol{j}_2$, $\boldsymbol{k}_2$ are the basis vectors of x-axis, y-axis, z-axis, and homogenous coordinate axis of S_2.

The relative velocity of the two gears in coordinate system S_2 is expressed as follows:

$$\boldsymbol{v}_2^{(12)} = [-(\omega_1-\omega_2)y_2 - a\omega_1\sin\phi_2]\boldsymbol{i}_2 + [(\omega_1-\omega_2)x_2 - a\omega_1\cos\phi_2]\boldsymbol{j}_2 \tag{2}$$

According to the geometry knowledge, in coordinate system S_2, the normal vector of given surface Σ_2 at a point can be represented as:

$$\boldsymbol{n}_2 = \frac{\partial\Sigma_2^2}{\partial u}\times\frac{\partial\Sigma_2^2}{\partial v} \tag{3}$$

Then, the meshing equation was achieved:

$$\boldsymbol{v}_2^{(12)}\cdot\boldsymbol{n}_2 = 0 \tag{4}$$

Then assuming that curve Γ_2 is on given surface Σ_2, and the equation of curve Γ_2 in movable coordinate system S_2 is

$$\Gamma_2^2 = x_2(u(\phi),v(\phi))\boldsymbol{i}_2 + y_2(u(\phi),v(\phi))\boldsymbol{j}_2 + z_2(u(\phi),v(\phi))\boldsymbol{k}_2 \tag{5}$$

where $x_2(u(\phi), v(\phi))$, $y_2(u(\phi), v(\phi))$, $z_2(u(\phi), v(\phi))$ are the scalar functions of ϕ.

After Γ_2 has been determined, the locus of Γ_1 in coordinate S_1 is given from the transformation matrices S_2 to S_1:

$$\Gamma_1^2 = \boldsymbol{M}_{12}\Gamma_2^2 = \boldsymbol{M}_{10}\boldsymbol{M}_{0p}\boldsymbol{M}_{p2}\Gamma_2^2 \tag{6}$$

where

$$\boldsymbol{M}_{12}=\boldsymbol{M}_{10}\boldsymbol{M}_{0p}\boldsymbol{M}_{p2}=\begin{bmatrix}\cos(\phi_1-\phi_2) & \sin(\phi_1-\phi_2) & 0 & -a\cos(\phi_1)\\ -\sin(\phi_1-\phi_2) & \cos(\phi_1-\phi_2) & 0 & a\sin(\phi_1)\\ 0 & 0 & 1 & 0\\ 0 & 0 & 0 & 1\end{bmatrix} \tag{7}$$

Then, the mathematical representations of conjugate curve Γ_1 in S_1 can be expressed as:

$$\begin{cases}\Gamma_1^2=\boldsymbol{M}_{12}\Gamma_2^2\\ \boldsymbol{v}_2^{(12)}\cdot\boldsymbol{n}_2^{12}=0\end{cases} \tag{8}$$

From the meshing equation and space meshing theory, it can be concluded that these two curves are also the contact paths of the pinion and gear, respectively.

2.2 Generation process of new tooth surface

The contact path which is conjugated to surface Σ_2 has been derived. In this section, the conjugate tooth surface is obtained according to the contact path. The generation of the surface is based on a family of continuously variable plane curves Γ_c, which is also the tooth profile. The construction process is as follows and shown in Fig. 2.

It is assumed that $\boldsymbol{\beta}_1^2$, $\boldsymbol{\alpha}_1^2$ and $\boldsymbol{\gamma}_1^2$ construct a coordinate system denoted by S_c and represent x-axis, y-axis and z-axis, where $\boldsymbol{\beta}_1^2$, $\boldsymbol{\alpha}_1^2$ and $\boldsymbol{\gamma}_1^2$ demonstrate the principal normal vector, tangent vector and binormal vector of curve Γ_2 in coordinate system S_1. Point P_t is set to be the coordinate origin. Then, curve Γ_c can be expressed as:

$$\Gamma(t)=(x(t)\quad 0\quad z(t)\quad 1)^{Tr} \tag{9}$$

where $x(t)$ and $z(t)$ are the scalar functions of t.

Thus, through coordinate transforming, the conjugate tooth surface in coordinate system S_1 can be expressed as:

$$S(\phi,t)=\boldsymbol{M}_c\Gamma(t) \tag{10}$$

where

$$\boldsymbol{M}_c=\begin{bmatrix}\boldsymbol{\beta}_1^2\cdot\boldsymbol{i}_1 & \boldsymbol{\alpha}_1^2\cdot\boldsymbol{i}_1 & \boldsymbol{\gamma}_1^2\cdot\boldsymbol{i}_1 & \\ \boldsymbol{\beta}_1^2\cdot\boldsymbol{j}_1 & \boldsymbol{\alpha}_1^2\cdot\boldsymbol{j}_1 & \boldsymbol{\gamma}_1^2\cdot\boldsymbol{j}_1 & \Gamma_1^2\\ \boldsymbol{\beta}_1^2\cdot\boldsymbol{k}_1 & \boldsymbol{\alpha}_1^2\cdot\boldsymbol{k}_1 & \boldsymbol{\gamma}_1^2\cdot\boldsymbol{k}_1 & \end{bmatrix} \tag{11}$$

$\boldsymbol{i}_1, \boldsymbol{j}_1, \boldsymbol{k}_1$ are the basis vectors of x-axis, y-axis, z-axis, and homogenous coordinate axis of S_1.

The tooth profile is intercepted by the tip and root cylinder surfaces of gear, thus, the gear is obtained and the illustration is shown in Fig. 3.

3. Mathematical Model of the Internal Gear Pair

3.1 Equation of helical internal gear

The tooth surface of an internal helical gear can be generated by the screw motion of an involute about the gear axis.[18] The equation of the internal gear tooth surface in coordinate system S2 can be expressed as:

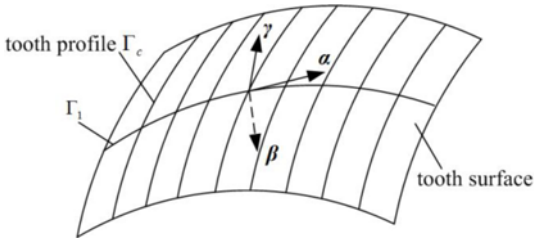

Fig. 2 Generation of tooth surface

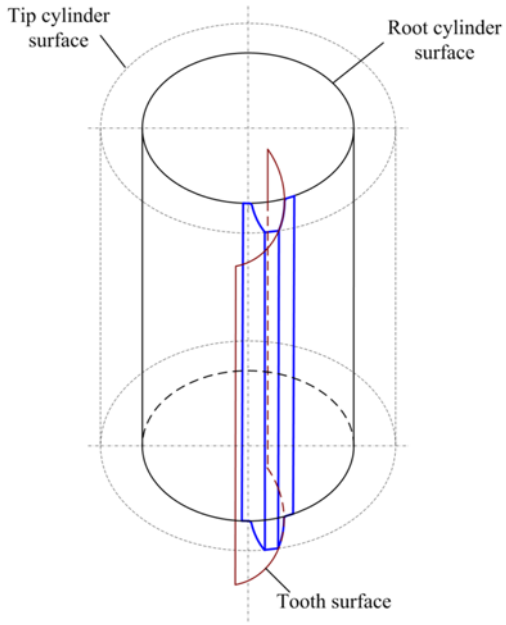

Fig. 3 Generation of tooth surface

$$\begin{cases}x_{\Sigma 2}=r\cos(\theta+\alpha)+r\theta\sin(\theta+\alpha)\\ y_{\Sigma 2}=r\sin(\theta+\alpha)-r\theta\cos(\theta+\alpha)\\ z_{\Sigma 2}=p\alpha\end{cases} \tag{12}$$

3.2 Selecting of the contact path

As for other gear pair which is point contact such as circular arc gear, the contact path is usually a circular helix. However, one of the features of the gear pair proposed in this paper is the contact path can be selectable as needed, including but not limited to circular helix, which brings more flexibility and diversity for gear designing.

As mentioned in section 2.1, curve Γ_2 is also the contact path of the gear pair and it is on given surface Σ_2, and the equation of curve Γ_2 is presented in Eq. (5). Generally, for parallel-axis gear transmission, the selected curve is within the range of the tooth root and top. The way of mesh is from one side of gear to the other side because of the point contact pattern, i.e., from the approach point to the recess point. There are tremendous paths connecting two points on a surface (Fig. 4). The shortest path is the geodesic.[19] In some cases, the mathematical expression of the geodesic on the surface may be too complex. Hence, a simple expression can be appointed to decrease the amount of calculation.

Curve Γ_2 on the tooth surface of the internal gear can be obtained by

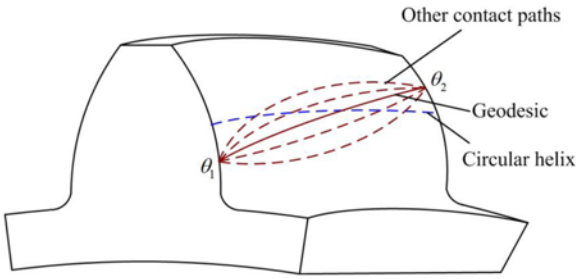

Fig. 4 Selecting of the contact path

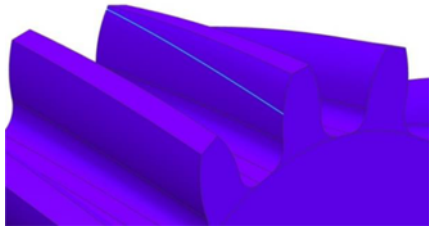

Fig. 5 Contact path in this paper

many ways, as mentioned in section 3.2. To make it simple, we assumed that there is a linear relationship between θ and α. The expression can be written as:

$$\alpha = k\theta + b \tag{13}$$

where $k = B / p(\theta_2\text{-}\theta_1)$, $b = \theta_1 B / p(\theta_2\text{-}\theta_1)$, the range of involute parameter θ is $\theta_1 \le \theta \le \theta_2$, θ_1, θ_2 are the initial value and final value of θ.

Then,

$$\Gamma_2^2 = \begin{cases} x_{\Gamma 2} = r\cos(\theta+\alpha) + r\theta\sin(\theta+\alpha) \\ y_{\Gamma 2} = r\sin(\theta+\alpha) - r\theta\cos(\theta+\alpha) \\ z_{\Gamma 2} = p\alpha \\ \alpha = k\theta + b \end{cases} \tag{14}$$

3.3 Equation of pinion tooth surfaces

According to Eq. (3), the normal vector of the tooth surface on point p_l, which is on the contact path, can be obtained as

$$\begin{cases} n_{x2} = -pr\theta\sin[(k+1)\theta + b] \\ n_{y2} = pr\theta\cos[(k+1)\theta + b] \\ n_{z2} = -r^2\theta \end{cases} \tag{15}$$

Then, the meshing equation is expressed as:

$$A\sin(\phi_2) + B\cos(\phi_2) = M \tag{16}$$

where

$\phi_1 = i_{12}\phi_2$, $A = i_{12}an_{x2}$, $B = i_{12}an_{y2}$, $M = (i_{12}-1)(x_2n_{y2} - y_2n_{x2})$.

Substituting Eqs. (7), (14), (15) and (16) into Eq. (8), the equation of conjugate curve Γ_1 in S_1 can be expressed as:

$$\begin{cases} x_{\Gamma 1} = x_{\Gamma 2}\cos((i_{12}-1)\phi_2) + y_{\Gamma 2}\sin((i_{12}-1)\phi_2) - a\sin(i_{12}\phi_2) \\ y_{\Gamma 1} = -x_{\Gamma 2}\sin((i_{12}-1)\phi_2) + y_{\Gamma 2}\cos((i_{12}-1)\phi_2) + a\sin(i_{12}\phi_2) \\ z_{\Gamma 1} = z_{\Gamma 2} \\ A\sin(\phi_2) + B\cos(\phi_2) = M \end{cases} \tag{17}$$

From section 2.2, quadratic curve tooth profile is applied in this internal gear pair. The tooth profile in S_c can be written as:

$$\Gamma(t) = (x_c, y_c, z_c, 1)^{Tr} = (k_1t^2 \quad 0 \quad k_1t \quad 1)^{Tr} \tag{18}$$

According to section 2, β_1^2, α_1^2 and γ_1^2 can be expressed as:

$$\begin{cases} n_{x\beta 2} = n'_{x2}\cos[(i_{12}-1)\phi_2] + n'_{y2}\sin[(i_{12}-1)\phi_2] \\ n_{y\beta 2} = -n'_{x2}\sin[(i_{12}-1)\phi_2] + n'_{y2}\cos[(i_{12}-1)\phi_2] \\ n_{z\beta 2} = n'_{z2} \end{cases} \tag{19}$$

$$\begin{cases} n_{x\alpha 2} = x'_{\Gamma 2}\cos[(i_{12}-1)\phi_2] + y'_{\Gamma 2}\sin[(i_{12}-1)\phi_2] \\ n_{y\alpha 2} = -x'_{\Gamma 2}\sin[(i_{12}-1)\phi_2] + y'_{\Gamma 2}\cos[(i_{12}-1)\phi_2] \\ n_{z\alpha 2} = z'_{\Gamma 2} \end{cases} \tag{20}$$

$$\begin{cases} n_{x\gamma 2} = n_{y\beta 2}n_{z\alpha 2} - n_{y\alpha 2}n_{z\beta 2} \\ n_{y\gamma 2} = n_{z\beta 2}n_{x\alpha 2} - n_{z\alpha 2}n_{x\beta 2} \\ n_{z\gamma 2} = n_{x\beta 2}n_{y\alpha 2} - n_{x\alpha 2}n_{y\beta 2} \end{cases} \tag{21}$$

Then, the equation of the pinion in S_1 is deduced as:

$$\Gamma_1^1 = \begin{cases} x_{\Sigma 1} = n_{nx\beta 2}x_c + n_{nx\alpha 2}y_c + n_{nx\gamma 2}z_c + x_{\Gamma 1} \\ y_{\Sigma 1} = n_{ny\beta 2}x_c + n_{ny\alpha 2}y_c + n_{ny\gamma 2}z_c + y_{\Gamma 1} \\ z_{\Sigma 1} = n_{nz\beta 2}x_c + n_{nz\alpha 2}y_c + n_{nz\gamma 2}z_c + z_{\Gamma 1} \end{cases} \tag{22}$$

where $\boldsymbol{n}_{nx\beta 2}$, $\boldsymbol{n}_{ny\alpha 2}$ and $\boldsymbol{n}_{nz\gamma}$ are the unit vectors of the principal normal vector, tangent vector and binormal vector, respectively and

$$\begin{cases} n_{nxi2} = \dfrac{n_{xi2}}{\sqrt{n_{xi2}^2 + n_{yi2}^2 + n_{zi2}^2}} \\ n_{nyi2} = \dfrac{n_{yi2}}{\sqrt{n_{xi2}^2 + n_{yi2}^2 + n_{zi2}^2}} \\ n_{nzi2} = \dfrac{n_{zi2}}{\sqrt{n_{xi2}^2 + n_{yi2}^2 + n_{zi2}^2}} \end{cases} \tag{23}$$

3.4 Equation of line of action

Line of action is defined as the set of the instantaneous contact points between two mating tooth profiles in the fixed coordinate system. Utilizing coordinate transformation from movable coordinate system S_2 to fixed coordinate system S_0, the equation of line of action can be obtained as:

$$\begin{cases} x = x_1\cos\phi_2 - y_1\sin\phi_2 - a \\ y = x_1\sin\phi_2 + y_1\cos\phi_2 \\ z = z_1 \end{cases} \tag{24}$$

4. Meshing Characteristics of the Internal Gear Pair

4.1 Motion simulation

The equation of the contact path is shown in Eq. (14). Unlike the

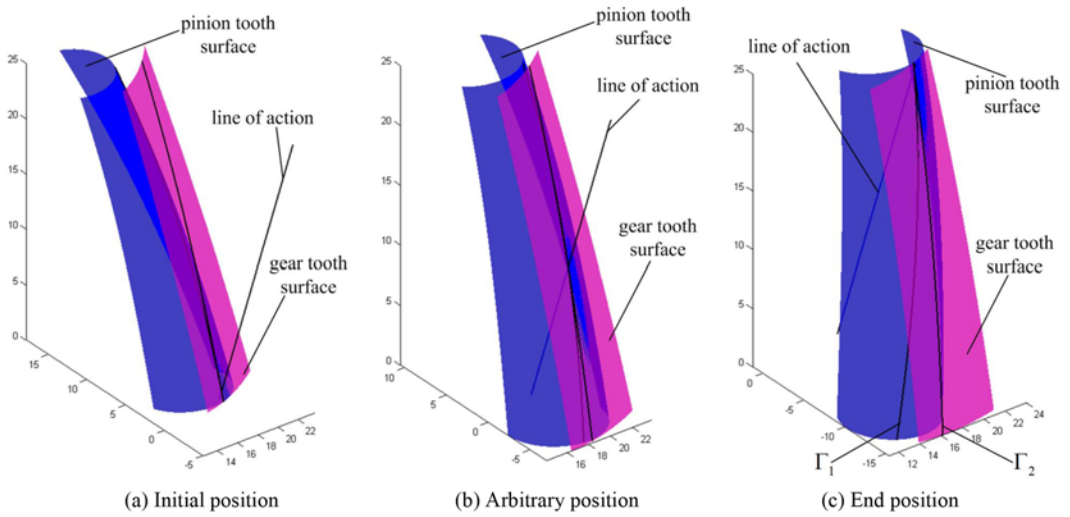

Fig. 6 Meshing schematic of tooth surfaces

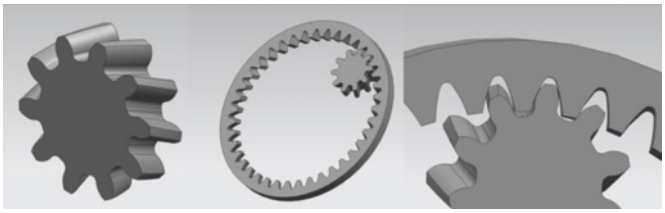

Fig. 7 Three-dimensional model of internal gear pair

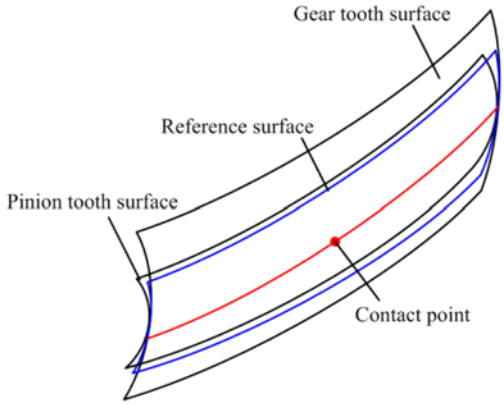

Fig. 8 Illustration of mesh

circular arc gear, the contact path in this paper shown in Fig. 5 is a combination of involute and circular helix.

As shown in Fig. 6, the simplified internal gear and pinion tooth surfaces are given. Line of action is depicted as a straight line. The engagement of tooth surfaces at the initial position is displayed in Fig. 6(a). When the gear pair rotates with an angular velocity, the tooth surfaces come in contact with each other in the contact point P_i. The meshing condition at arbitrary position is described in Fig. 6(b). The engagement of tooth surfaces at the end position is displayed in Fig. 6(c). During the transmission process, the internal gear and pinion tooth surfaces mesh in point contact. The instantaneous contact point of tooth surfaces is always on the line of action. The locus of the contact point on the pinion and internal gear are Γ_1 and Γ_2, respectively, i.e. the contact paths.

The tooth surface of the pinion can be constructed from Eq. (22). By using MATLAB and solid modeling software UG, a three dimensional model of the gear drive was established as shown in Fig. 7.

4.2 Adaptability to center distance variation

It is one of the advantages of the involute gear that the instantaneous transmission ratio remains unchanged, while center distance of the gear pair changes slightly. The proposed internal gear transmission also can adapt the change of the center distance due to uniqueness of the contact path. As shown in Fig. 8, according to Ref. 20, the contact path on the pinion Γ_1 is also a curve which is on an involute surface. Assuming that the involute surface is used as the reference surface which is engaged with the gear surface, then, the mesh of the proposed gear pair can be regarded as that of two involute gears.

As mentioned in section 4.1, the contact path of the internal gear pair is a combination of involute and circular helix and the projection on the gear end-face is a segment of involute. Therefore, the theoretical explanation is similar to that of the involute gear. Fig. 9(a) depicts the changes of the actual meshing section on line of action under the cases of increased center distance. In the case of standard center distance, the centers of the pinion and gear are located on the points O_1 and O_2, respectively. The theoretical meshing area is N_1N_2, and thick black line is the actual track. The entire contact traces within this range are involved in the mesh. Assuming that the gear is fixed and the center of the pinion moves from O_2 up to O'_2 along the center line of two gears. It can be seen that the meshing angle, line of action, and the node position also change. The theoretic mating area is now $N'_1N'_2$, and the actual track is the thick blue line. However, the base circles remain unchanged, and the common normal line is still tangent to the two base circles and still goes through the pitch point P.

In the case of reduced center distance which is shown in Fig. 9(b), in a similar way, the center of the pinion moves from O_2 down to O'_2 along the center line of two gears. The meshing angle, line of action, and the node position also change. The theoretic mating area is now N'_1

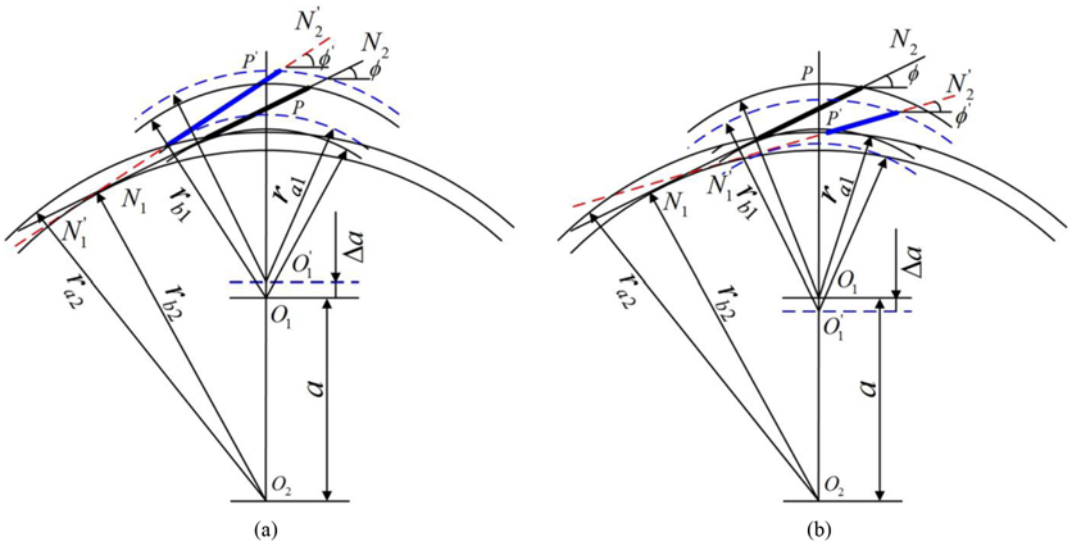

Fig. 9 Changes of center distance: (a) increased center distance; (b) decreased center distance

Table 1 Geometrical parameters of the gear drive

Normal module, m_n	2mm
Pressure angle on pitch circle, α	20°
Teeth number of pinion, z_1	18
Teeth number of gear, z_2	267
Tooth width, B	15
Independent variable range of curve, θ	[0.3534,0.6461] rad
Hand of helix (pinion and internal gear)	Right-hand
Helical angle	22.147°

Table 2 Material and heat treatment of the gear pair

	Material	Heat treatment	Hardness
Pinion	05Cr15Ni5Cu4Nb	solution treatment	HRC41~45
Internal gear	42CrMo	hardening and tempering	HRC 35~39

N'_2, and the actual track is the thick blue line and the transmission ratio is also unvaried. Therefore, for the new internal gear pair, no matter the center distance increases or vise versa, the transmission ratio remains unchanged and equals to the ratio of r_{b2} to r_{b1}. Therefore, the contact path can inherit the characteristic of the involute surface and adapt the center distance variation.

4.3 Prototype manufacturing

According to the mathematical model, the gear pair is manufactured. With the development of technology, the manufacture of complicated surface can be realized.[21] Considering the processing method and stability of the machine, the pinion is manufactured by using 5-axis machining center, DMU 60. It is of good working accuracy and operability. The processing technique of the involute gear has been well developed over the years. For internal gears, gear shaping is the common method due to its high production rates. In this paper, the internal gear is manufactured by grinding which is of high accuracy. The geometrical parameters and the heat treatment of gear pair are given in Tables 1 and 2, respectively. Fig. 10 shows the pinion and the internal gear which have been completed processing.

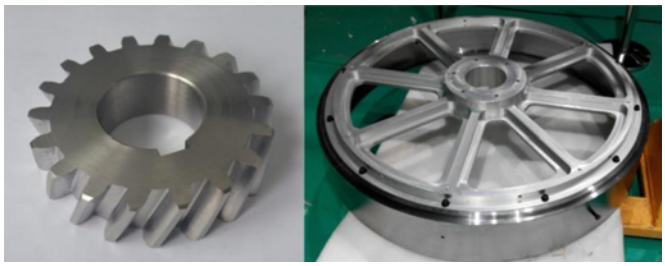

Fig. 10 The pinion and the internal gear

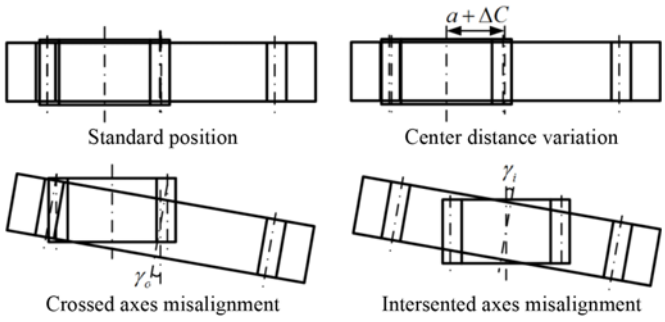

Fig. 11 Illustration of three types of assembly errors

5. Tooth Contact Analysis and Numeral Examples

5.1 Tooth contact analysis and kinematic error

It is unavoidable that elastic deformation and assembly errors such as center distance variation and axial misalignment take place in the process of gear transmission. In this section, the tooth contact analysis model is established to analyze the sensitivity of assembly errors of the proposed gear pair. With the mathematical models of gears and TCA technique,[22] the locations of contact points and the contact pattern of mating toot surfaces for various assembly cases are determined. The aim is to provide theoretic fundament for further research on transmission characteristics. Fig. 11 illustrates the three types of assembly errors and

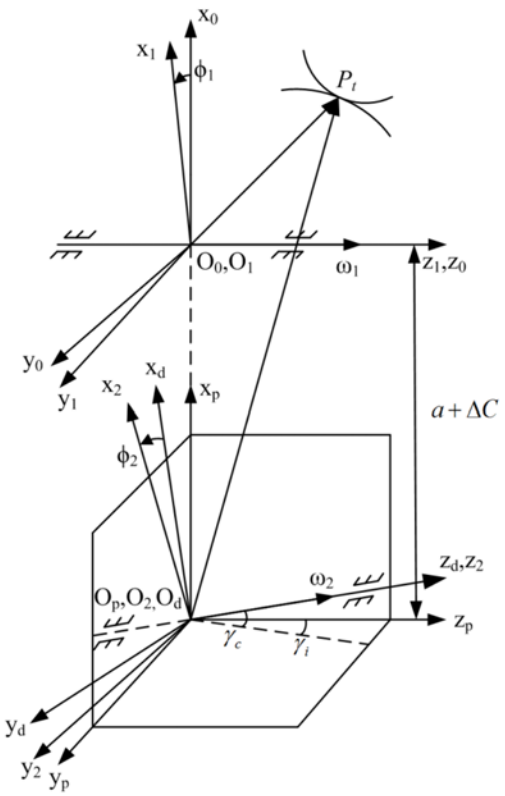

Fig. 12 Coordinate systems for tooth contact analysis

the coordinate systems are shown in Fig. 12.

Based on the coordinate systems in section 2.1, $S_d(O_d\text{-}x_d,y_d,z_d)$ is the auxiliary coordinate system for simulating the assembly errors between the pinion and internal gear, including the internal gear center distance variation ΔC, crossed axes misalignment $\Delta\gamma_c$ and intersected axes misalignment $\Delta\gamma_i$. By applying the coordinate transformations method, the tooth surface equations and unit normals of the pinion and internal gear can be represented in the fixed coordinate system S_0 and $\mathbf{M}_{pd}$ represents the transformation matrix from system d to p and can be expressed as:

$$\boldsymbol{M}_{pd} = \begin{bmatrix} \cos\phi_2\cos\gamma_c & -\sin\phi_2\sin\gamma_i & -\cos\phi_2\sin\gamma_c & -a-\Delta C \\ -\sin\phi_2\sin\gamma_c\sin\gamma_i & & -\sin\phi_2\cos\gamma_c\sin\gamma_i & \\ \sin\phi_2\cos\gamma & \cos\phi_2\cos\gamma_i & \cos\phi_2\cos\gamma_c\sin\gamma_i & 0 \\ +\cos\phi_2\sin\gamma_c\sin\gamma_i & & -\sin\phi_2\sin\gamma_c & \\ \sin\gamma_c\cos\gamma_i & -\sin\gamma_i & \cos\gamma_c\cos\gamma_i & 0 \\ 0 & 0 & 0 & 1 \end{bmatrix} \quad (25)$$

According to the TCA theory, at the contact point, the position vectors and their unit normals of both the internal gear and pinion tooth surfaces should be the same due to the tangency of the two gear tooth surfaces. Therefore, the following equations can be derived.

$$\begin{cases} \boldsymbol{M}_{01}\Gamma_1^1 = \boldsymbol{M}_{0p}\boldsymbol{M}_{pd}\Gamma_2^d \\ \boldsymbol{M}_{01}\boldsymbol{n}_1^1 = \boldsymbol{M}_{0p}\boldsymbol{M}_{pd}\boldsymbol{n}_2^d \end{cases} \quad (26)$$

where $\boldsymbol{n}_1^1$ and $\boldsymbol{n}_2^d$ are the unit normals of pinion and internal gear in coordinate systems S_1 and S_d, respectively.

Also, the kinematic error of the gear pair can be expressed as:

$$\Delta\phi_2 = \phi_1 - \frac{z_1}{z_2}\phi_2 \quad (27)$$

where ϕ_2 is chosen as the input variable and ϕ_1 can be determined according to Eq. (26).

5.2 Illustrative numeral examples and discussions

In this section, the effects of assembly error conditions on contact paths and kinematic errors are discussed according to the geometrical parameters in Table 1. The analysis is focused on the gear pair meshing under four specific assembly errors: center distance variation, crossed axes misalignment, intersected axes misalignment and mixed conditions of these assembly errors.

Example 1: Gear pair is meshing with no assembly errors, i.e., $\Delta C = 0$, $\gamma_i = 0^o$, $\gamma_c = 0^o$. The results of TCA are shown in Fig. 13(a).

In this example, the blue line is the ideal contact path generated according to the equations in section 3.3. It is noted that all the contact points of both the pinion and internal gear are located on the ideal contact path and no kinematic error is induced.

Example 2: If the gear pair is meshing under a center distance variation, i.e., $\Delta C = 0.5$ mm, $\gamma_i = 0^o$, $\gamma_c = 0^o$ and the results are shown in Fig. 13(b).

Fig. 13(b) shows that the contact points of the pinion are located on the ideal contact path, while that of the internal gear changes a little along the radial direction. In addition, no kinematic error occurs during the transmission process.

Example 3: If the gear pair is meshing under a crossed axes misalignment, i.e., $\Delta C = 0$, $\gamma_i = 0^o$, $\gamma_c = 0.3^o$ and the results are shown in Fig. 13(c).

In this example, the gear pair still meshes with point contact pattern and no edge contact occurs. The yellow line is the real contact path. Compared with the ideal contact path, the distributions of contact points of both the pinion and internal gear have small changes, and the maximum kinematic error is 22 arc sec.

Example 4: If the gear pair is meshing under an intersected axes misalignment, i.e., $\Delta C = 0$, $\gamma_i = 0.3^o$, $\gamma_c = 0^o$ and the results are shown in Fig. 13(d).

As shown in Fig. 13(d), compared with the example of crossed axes misalignment, the kinematic error is much less and the maximum kinematic error is 9.8 arc sec. Also, no edge contact occurs during the transmission process.

Example 5: If the gear pair is meshing under mixed conditions of these assembly errors, i.e., $\Delta C = 0.5$ mm, $\gamma_i = 0.3^o$, $\gamma_c = 0.3^o$ and the results are shown in Fig. 13(e).

Compared with all the five examples, the change of the contact path is the largest and the kinematic error is the highest, of which maximum value is 35 arc sec.

On the whole, the locations of the contact points of the pinion do not change under center distance variation, while that of the internal gear changes at a small range. The location of both of the gear and pinion changes under axes misalignment. No kinematic error occurs under center distance variation. Little kinematic error occurs under axes misalignment. The kinematic error induced by crossed axes misalignment is larger than that induced by intersected axes

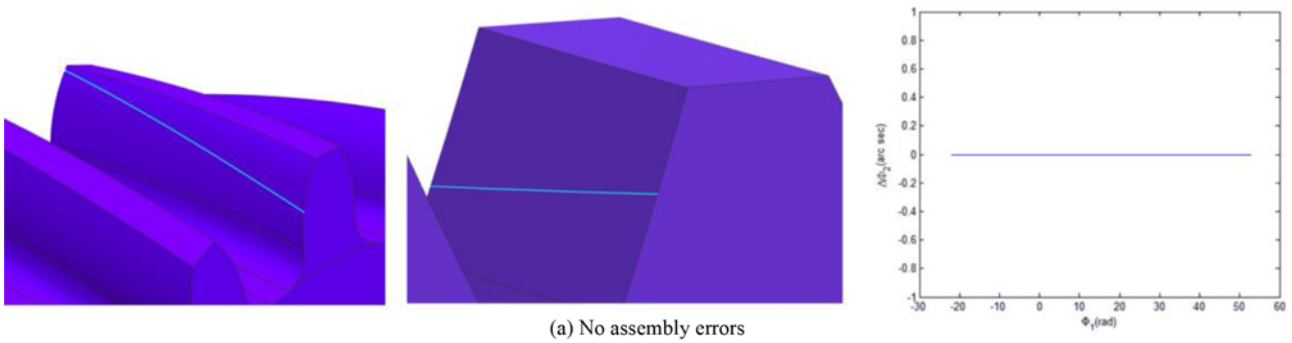

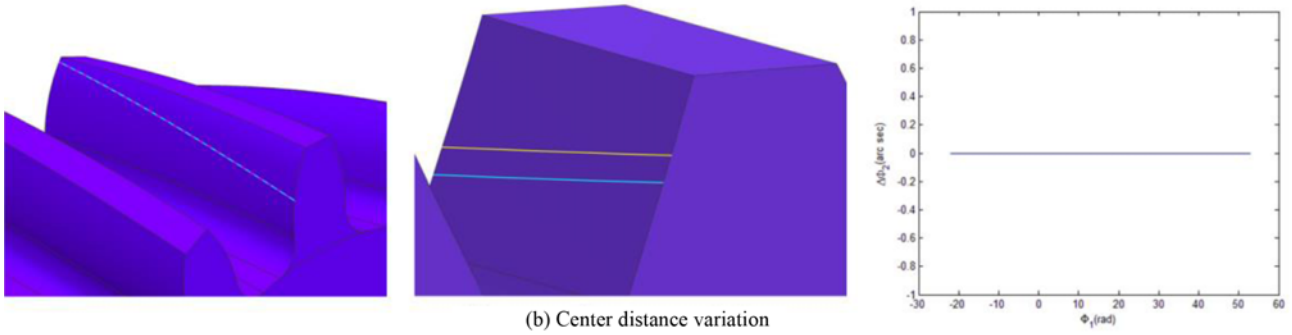

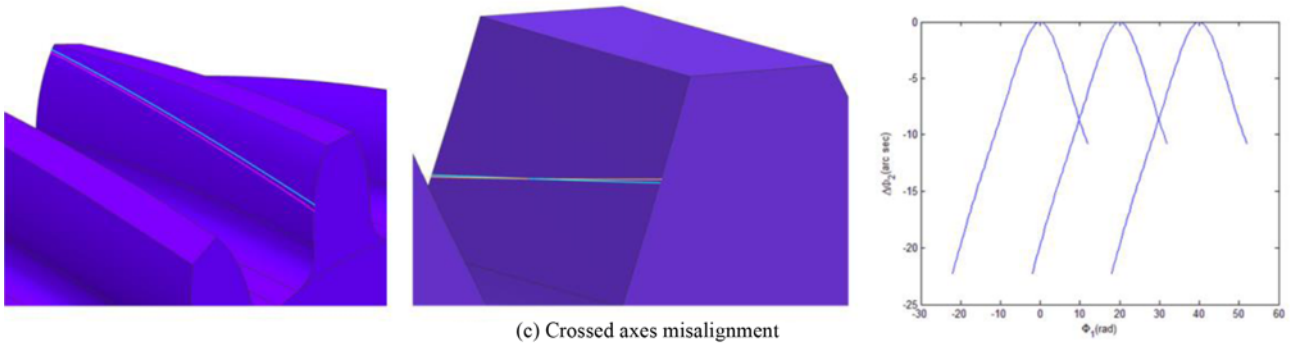

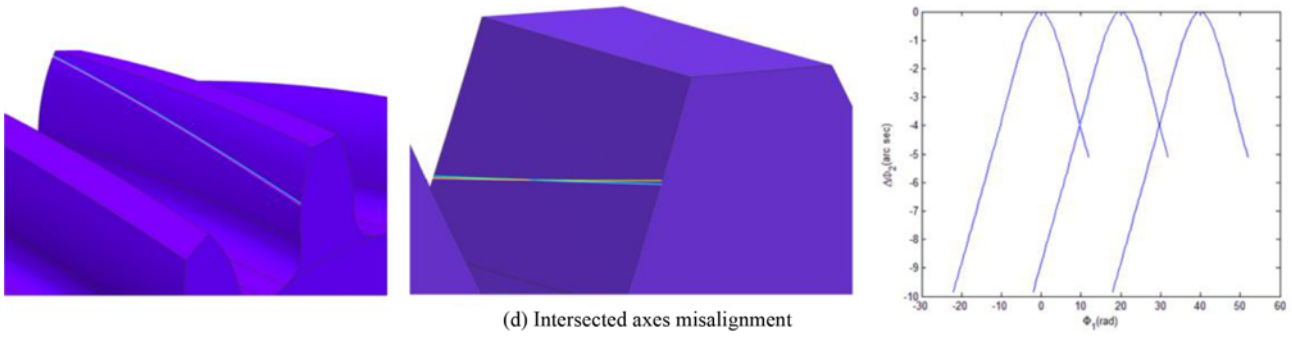

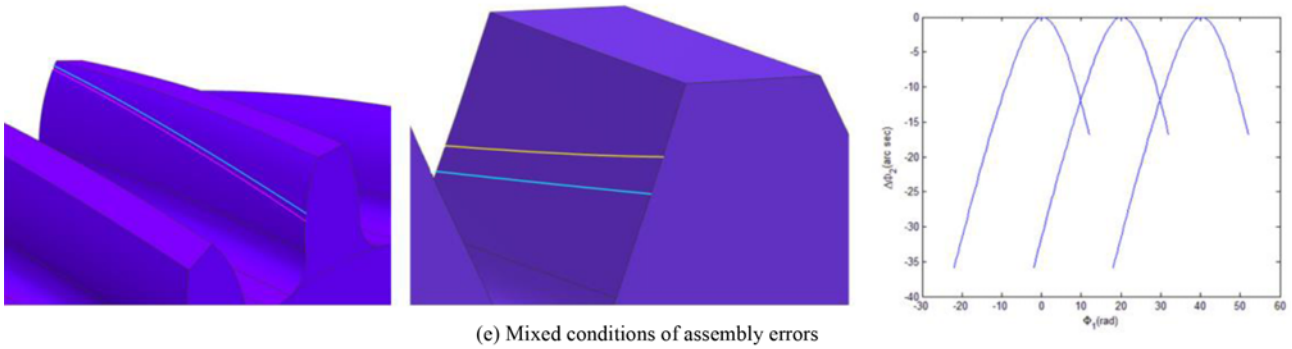

Fig. 13 Location of contact points and kinematic error

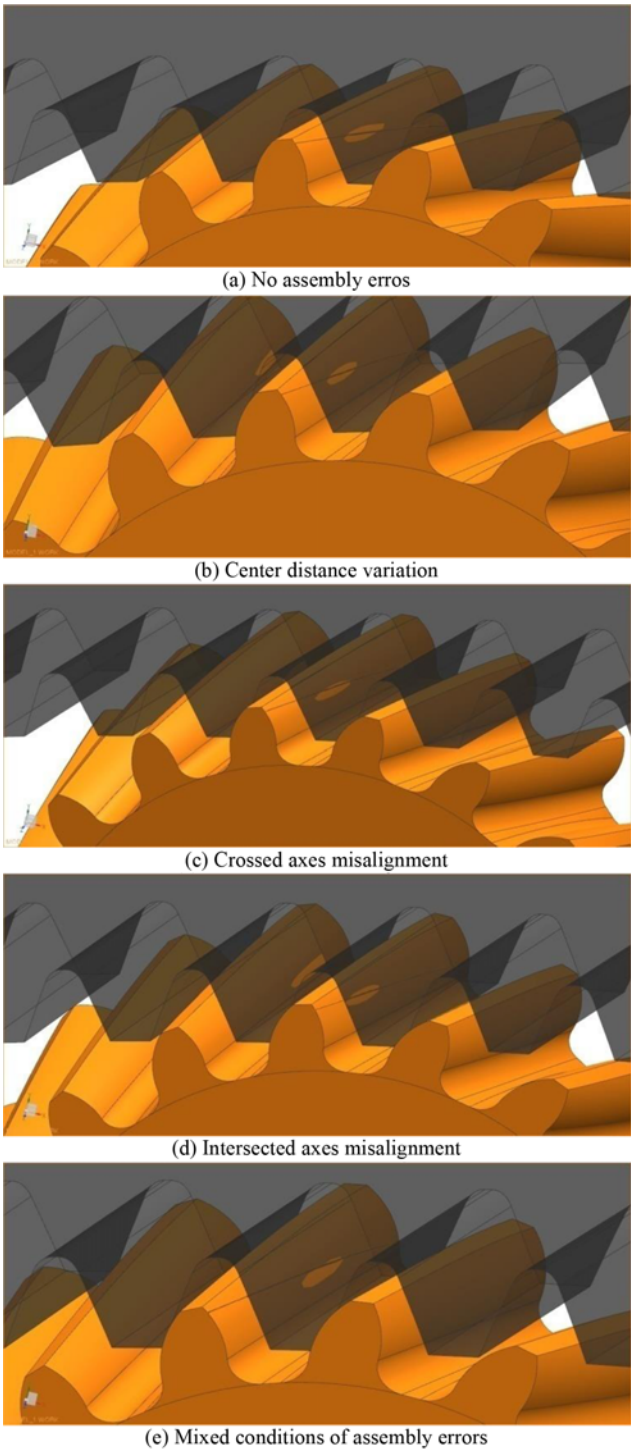

Fig. 14 Motion simulation

misalignment and is the largest under mixed conditions of these assembly errors, which should be avoided in using the type of gear pair. It is worth emphasizing that gear backlash changes under assembly errors and interference may occur when it is too small. To avoid interference, one effective way is to reduce the tooth thickness appropriately, which can increase backlash.

5.3 Simulation analysis

Based on the three dimensional models in Fig. 14, a computerized simulation of the meshing process is conducted in CAD software to demonstrate the contact path under different assembly errors. The black line is the ideal contact path and the contact ellipse can be clearly seen. The following characteristics are observed: (1) The gears can transmit rotational motion with a constant gear ratio and fulfill continuous transmission between mating tooth surfaces. (2) No meshing interference is observed between tooth surfaces. (3) The contact ellipse is displaced from the ideal contact path under crossed axes misalignment, intersected axes misalignment and mixed conditions of assembly errors while it coincides with the ideal contact path under no assembly errors and center distance variation, which validates the theoretical analysis in section 5.2.

Fig. 15 Test rig

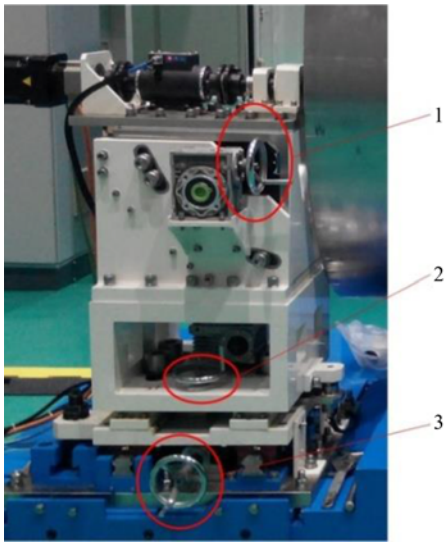

Fig. 16 Handwheels on the test rig

6. Performance Experiment

6.1 Test rig

To investigate the transmission performance of the gear pair with assembly errors, a gear drive test rig shown in Fig. 15 is designed and could be used to investigate the transmission efficiency of this new gear drive. To simulate the working conditions of center distance variation and axial misalignment, the ball screw pair is applied and handwheels labeled 1, 2 and 3 as illustrated in Fig. 16 are used to adjust intersected axes misalignment, crossed axes misalignment and center distance variation, respectively.

6.2 Test procedure

Considering the point contact pattern of the internal gear pair, a running-in process is carried out to expand the contact area and modify the tooth surface for increasing the load capacity and reducing noise and vibration. In general, when the contact area is large, the load capacities of the gear are high. The running-in process lasts for 8 hours. The first 4 hours run with an input speed of 60 rpm, and the next 4 hours run with an input speed of 60 rpm and an output torque of 60 Nm. After 8 hours running-in process, the gear pair is considered to be under an ideal contact situation.

To investigate the transmission efficiency with no assembly errors, the test rig is operated in different motor speeds (30 rpm, 60 rpm, 90 rpm, and 120 rpm) and different output torsional moments (30 Nm to 100 Nm). The system is stopped after 80 hours.

To investigate the transmission efficiencies with assembly errors, the test rig is operated with: (1) ΔC = 0.5 mm, γ_i = 0°, γ_c = 0°; (2) ΔC = 0, γ_i = 0°, γ_c = 0.3°; (3) ΔC = 0, γ_i = 0.3°, γ_c = 0°; (4) ΔC = 0.5 mm, γ_i = 0.3°, γ_c = 0.3°. The motor speed is 60 rpm and output torsional moment is 30 Nm to 100 Nm. Each working condition lasts for 20 hours.

6.3 Results and discussions

6.3.1 Contact path

Fig. 17(a) shows the theoretical contact path. The blue line is the theoretical contact path with no assembly errors and the red line the theoretical contact path with assembly errors. After the experiments, the contact path can be clearly seen in Figs. 17(b) and (c). The contact paths look similar and they are both a curve from tooth addendum to tooth dedendum, which is consistent with the theoretical analysis. Due to the elastic deformations, the contact point will spread over a small area and can be seen by using scanning electron microscope. In Figs. 17(b) and (c), the area between the red lines is the contact region. Compared with the two contact regions, the region with assembly errors is larger than that with no assembly errors, which is because of the complexity of the working conditions and the change of contact path of different situations.

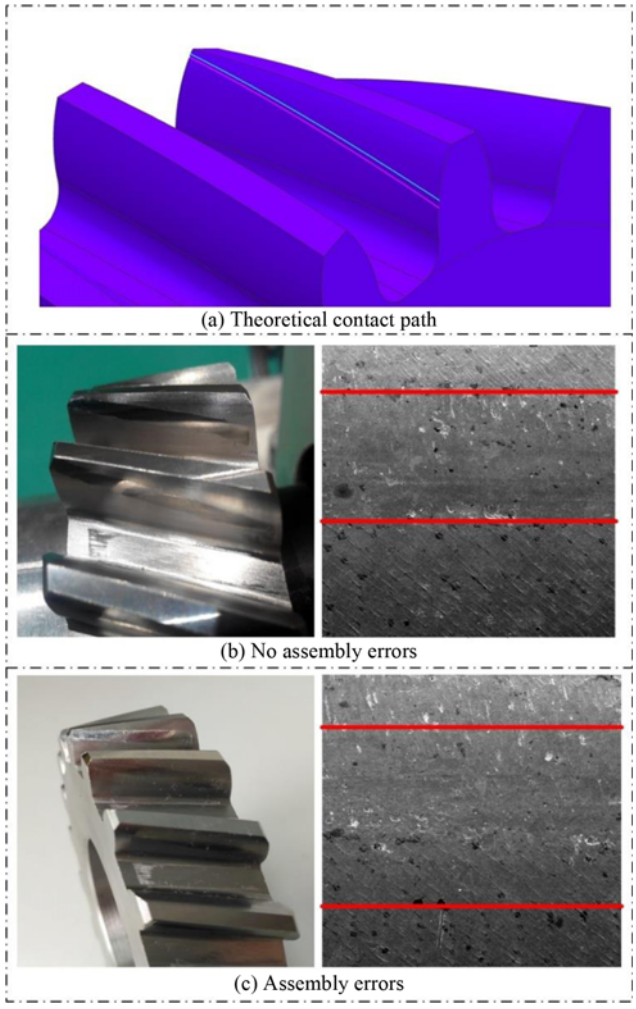

Fig. 17 Contact path

6.3.2 Efficiency

Input torque T_i, input shaft speed n_i, output values T_o and shaft speed n_o are measured by torque and rotational speed transducers. Transmission efficiency can be calculated as $\eta = T_o\ n_o\ /\ T_i\ n_i$.

The transmission efficiency of the gear pair with and without assembly errors is shown in Fig. 18. It can be concluded that:

(1) When the torque is constant, the efficiency increases with the rotational speed. Similarly, when the rotational speed is constant, the efficiency increases with the torque.

(2) The efficiency of the gear pair with standard center distance is stable at a range about 97% to 98.3% while the motor speed is 60 rpm.

(3) The efficiency with assembly errors is almost the same as that with standard center distance and the deviation is between 0.3%.

Based on the experiment result, the gear pair is expected to have excellent advantages: the efficiency is high and assembly errors have no influence on efficiency. Due to this property, this kind of gear pair can be applied under certain circumstances where assembly errors occur.

6.3.3 Wear

To investigate the roughness of the tooth surfaces, pinions are analyzed by scanning electron microscope after the experiment. One tooth is cut off from the two pinions respectively and scanned by scanning electron microscope to observe surface topography at a magnification of 400 times and the results are shown in Fig. 19. After the experiment, mild abrasive wear occurs. However, in terms of the roughness of tooth surface, the contact regions of both pinions become smoother than the uncontact region. This observation is attributed to two reasons: (1) the low sliding ratio of the gear pair is low since the range of the contact path is near the area of pitch line, where sliding ratio is zero. (2) The run time is not too much. Compared with the contact regions of both pinions, there is nearly no difference.

To evaluate the roughness of the tooth surface more precisely, wear depth of two pinions are measured by measuring center[6] and the conclusion is shown is Fig. 20. It is noted that: (i) wear increases along the tooth addendum and tooth dedendum and the maximum wear occurs on the tooth root where mesh begins with the pinion. There is no wear at pitch line as the sliding ratio is zero at this point. (ii) wear range of pinion with assembly errors is a little larger than that with no assembly errors and the difference in wear depth values is small, which is because the gears can mesh correctly under assembly errors.

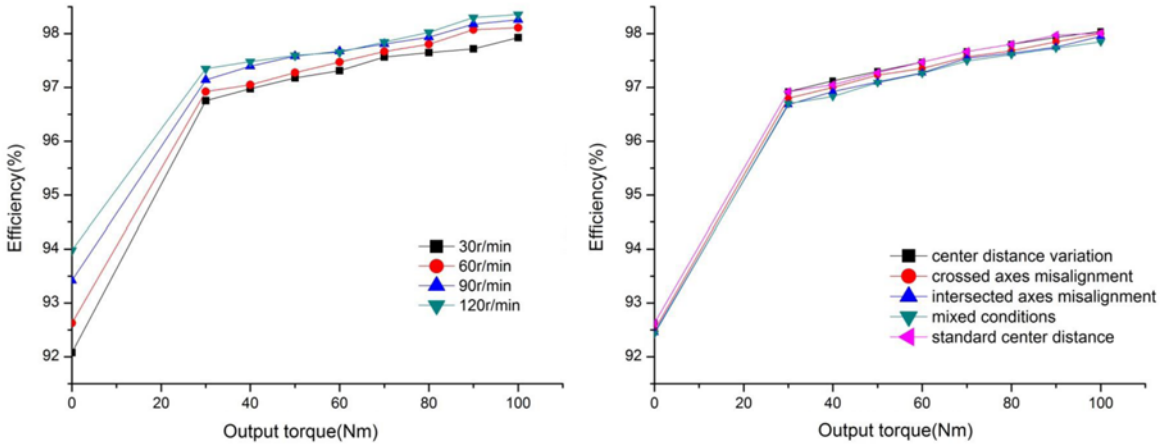

Fig. 18 Transmission efficiency with: (a) no assembly errors; (b) assembly errors

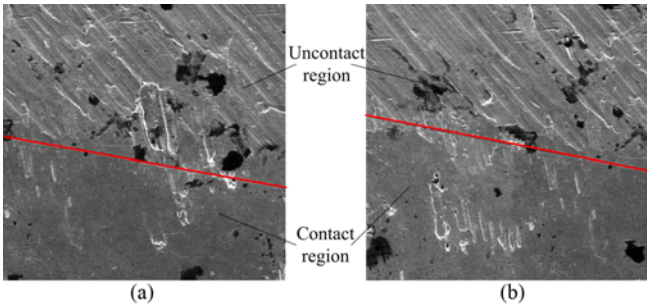

Fig. 19 Surface topography of pinion with: (a)no assembly errors; (b) assembly errors

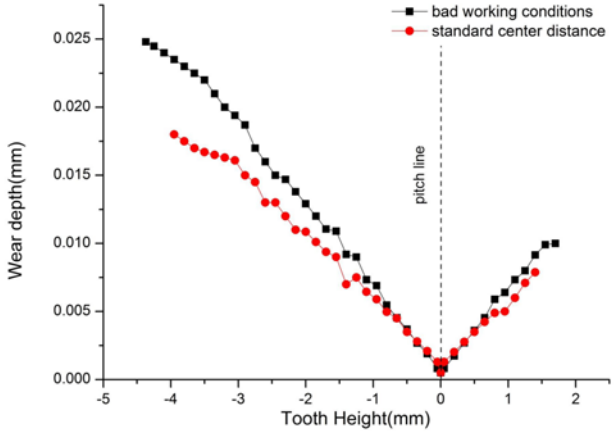

Fig. 20 Variation of wear depth

7. Conclusions

In this paper, an internal helical gear pair with point contact pattern based on the space meshing theory is proposed. The generation principle and mathematical model of the internal gear pair is presented. The gear pair consists of an internal gear and a pinion with quadratic curve tooth profile. Particularly, the contact path of the tooth surface is selectable, which is able to inherit the characteristic of the surface and provides more flexibility and diversity for gear designing. The motion simulation and adaptability to center distance error of the internal gear pair are discussed. Based on the mathematical model and TCA method, the locations of contact points and kinematic errors are determined under different center distance variations and axial misalignments. The simulated results of five numeral examples lead to the following conclusions:

(1) The contact pattern of this type of gear pair is point contact no matter with or without assembly errors.

(2) The location of the contact points of the pinion doesn't change under center distance variation, while that of the internal gear changes at a small range. Compared with the ideal contact path, the locations of both of the gear and pinion do not change much under crossed axes misalignment and intersected axes misalignment.

(3) No kinematic error occurs with no assembly errors and under center distance variation and little kinematic error induced by crossed axes misalignment is larger than that induced by intersected axes misalignment. Mixed conditions of these assembly errors can cause the largest kinematic error, but the value is still small.

(4) No edge contact occurs under any assembly error condition.

(5) Motion simulation and experiment study are performed and the result is consistent with the theoretical analysis. The efficiency with assembly errors keeps almost the same as that with no assembly errors, which is because the gears can mesh correctly under assembly errors.

(6) The internal gear pair has lower sensitivity to assembly error and lower assembly precision is needed in the application, which is the prominent feature of this type of gear pair.

ACKNOWLEDGEMENT

This research is supported by National Natural Science Foundation of China (Grant No. 51605049 and 51575062). The authors of the paper would like to appreciate their financial support of the research projects.

REFERENCES

1. Peeters, J. L., Vandepitte, D., and Sas, P., "Analysis of Internal Drive

Train Dynamics in a Wind Turbine," Wind Energy, Vol. 9, Nos. 1-2, pp. 141-161, 2006.

2. Shao, R., Jia, P., and Dong, F., "Dynamic Characteristics of Cracked Gear and Three-Dimensional Crack Propagation Analysis," Proceedings of the Institution of Mechanical Engineers, Part C: Journal of Mechanical Engineering Science, Vol. 227, No. 6, pp. 1341-1361, 2013.
3. Zhang, Y. S., Hu, X. H., Liu, Y. B., Liu, X. H., and Chen, L., "The Study of Straight Conjugate Internal Meshing Gear Pump," Machinery Design and Manufacture, No. 6, pp. 138-139, 2010. (in Chinese)
4. Xu, W. B., "Study on the Internal Meshing and Transmission of Double-Circular-Arc Gear," Zhengzhou Research Institute of Mechanical Engineering, pp. 20-38, 2012. (in Chinese)
5. Kahraman, A. and Vijayakar, S., "Effect of Internal Gear Flexibility on the Quasi-Static Behavior of a Planetary Gear Set," Journal of Mechanical Design, Vol. 123, No. 3, pp. 408-415, 2001.
6. Tunalioğlu, M. Ş. and Tuç, B., "Theoretical and Experimental Investigation of Wear in Internal Gears," Wear, Vol. 309, Nos. 1-2, pp. 208-215, 2014.
7. Litvin, F. L., Fuentes, A., Gonzalez-Perez, I., Carvenali, L., Kawasaki, K., and Handschuh, R. F., "Modified Involute Helical Gears: Computerized Design, Simulation of Meshing and Stress Analysis," Computer Methods in Applied Mechanics and Engineering, Vol. 192, Nos. 33-34, pp. 3619-3655, 2003.
8. He, D. W. and Fang, Z. D., "Air Cylindrical Gear Tooth Modification to Optimize the Design," Journal of Northwestern Polytechnical University, No. 10, pp. 323-328, 1992. (in Chinese)
9. Han, X., Hua, L., Deng, S., and Luo, Q., "Influence of Alignment Errors on Contact Pressure during Straight Bevel Gear Meshing Process," Chinese Journal of Mechanical Engineering, Vol. 28, No. 6, pp. 1089-1099, 2015.
10. Wang, H., Deng, X., Kai, X., Yang, J., and Su, J., "Load Tooth Contact Analysis (LTCA) of Helical Gears Using Topographic Modification and Installation Errors," Journal of Northwestern Polytechnical University, Vol. 32, No. 5, pp. 781-786, 2014. (in Chinese)
11. Wang, J., Wang, J., and Lim, T. C., "Influence of Assembly Error and Bearing Elasticity on the Dynamics of Spur Gear Pair," Proceedings of the Institution of Mechanical Engineers, Part C: Journal of Mechanical Engineering Science, Vol. 230, No. 11, pp. 1805-1818, 2016.
12. Tang, J., Chen, C., and Pu, T., "LTCA Analyses of Spiral Bevel Gears with Machining Errors, Assembly Errors, Axial Deformation and Bearing Stiffness," Journal of Mechanical Transmission, Vol. 34, No. 5, pp. 5-16, 2010. (in Chinese)
13. Shen, Y., Fang, Z., Zhao, M., and Wei, B., "Meshing Analysis of a Face-Gear Drive with a Spur Pinion Considering Tooth Edge Contact," Mechanical Science and Technology for Aerospace Engineering, Vol. 28, No. 8, pp. 1096-1100, 2009. (in Chinese)
14. Litvin, F. L., Chen, N. X., Lu, J., and Handschuh, R. F., "Computerized Design and Generation of Low-Noise Helical Gears with Modified Surface Topology," Journal of Mechanical Design, Vol. 117, No. 2, pp. 254-261, 1995.
15. Chen, Y.-C. and Tsay, C.-B., "Contact Ratios and Transmission Errors of a Helical Gear Set with Involute-Teeth Pinion and Modified-Circular-Arc-Teeth Gear," JSME International Journal Series C Mechanical Systems, Machine Elements and Manufacturing, Vol. 44, No. 3, pp. 867-874, 2001.
16. Karpat, F. and Ekwaro-Osire, S., "Influence of Tip Relief Modification on the Wear of Spur Gears with Asymmetric Teeth," Tribology Transactions, Vol. 51, No. 5, pp. 581-588, 2008.
17. Wang, W.-S. and Fong, Z.-H., "Tooth Contact Analysis of Longitudinal Cycloidal-Crowned Helical Gears with Circular Arc Teeth," Journal of Mechanical Design, Vol. 132, No. 3, Paper No. 031008, 2010.
18. Zhang, Z., "Involute Cylindrical Gear Transmission," China Machine Press, pp. 103-106, 2001. (in Chinese)
19. Zhao, J., Xin, S., Liu, Y., Wang, X., Wu, Z., et al., "A Survey on the Computing of Geodesic Distances on Meshes," Scientia Sinica Informationis, Vol. 45, No. 3, pp. 313-335, 2015.
20. Chen, B., Liang, D., Peng, S., and Zhang, J., "Analysis on Geometric and Contact Characteristics of Tubular Meshing Tooth Surfaces for Conjugate-Curve Gears," Journal of Xi'an Jiaotong Univertisy, Vol. 49, No. 3, pp. 85-94, 2015.
21. Wei, J., Zhang, Q., Xu, Z., and Lyu, S., "Study on Precision Grinding of Screw Rotors Using CBN Wheel," International Journal of Precision Engineering and Manufacturing, Vol. 11, No. 5, pp. 651-658, 2010.
22. Li, T. and Pan, C., "Mathematical Models of Grinding Manufacture and Tooth Contact Analysis of Spherical Gears," Science in China Series E: Technological Sciences, Vol. 52, No. 10, pp. 2823-2830, 2009.